EXPERIMENTAL FACILITIES FOR ELECTRIC PROPULSION TESTING*

Wilhelmus M. Ruyten**, Verlin J. Friedly†, Xiaohang Peng‡ and Dennis Keefer§

University of Tennessee-Calspan
Center for Advanced Space Propulsion
UTSI Research Park
Tullahoma, TN 37388

ABSTRACT

Experimental facilities for electric propulsion testing at the University of Tennessee Space Institute, jointly operated by the Center for Advanced Space Propulsion, include a cryogenically cooled, computer-controlled, 9 ft diameter by 20 ft long vacuum chamber, capable of maintaining a baseline pressure of 10^{-7} Torr, a 30 cm diameter ion thruster, and laser diagnostic and electrical diagnostic instrumentation. These facilities are described here in some detail, with emphasis on the measurement of ion thruster parameters such as neutral and ion densities, temperature, and velocity in the exhaust, as well as plasma potential and electron temperature.

I. INTRODUCTION

Although electric propulsion devices such as ion thrusters and arcjets have been around for many years, and much ground-based testing has been performed, critical issues remain unsettled, limiting the deployment of these devices in actual space missions. With regard to ion thrusters, one of these critical issues is the erosion of the extraction grids [1]. Ground based studies of ion thrusters indicate that this erosion is a serious issue indeed, but that the erosion in ground-based tests overestimates the erosion that would take place in an actual space flight due to the inability to maintain a space-like vacuum in a ground test.

Two parallel developments at the Center for Advanced Space Propulsion are underway that might resolve the issue of erosion rates in an ion thruster operated in a space-like vacuum. One of these is the completion of a large, cryogenically cooled vacuum facility. While this facility may not actually reach the ultrahigh vacuum of space for all operating conditions of the thruster, the background pressure will be sufficiently low to allow a reasonable extrapolation of the results to those for a space vacuum. The other development, described in detail in the accompanying paper [2], is that of a numerical code capable of predicting erosion rates for a wide range of operating parameters for the thruster. However, in order for this numerical code to provide not only qualitative but also quantitative results, accurate values for a number of experimental parameters must be obtained, for example, plasma potential, electron temperatures, and ion velocities in various regions of the thruster flow.

This paper describes the experimental facilities that will be used to obtain these thruster data. The vacuum facility is described in Section II. Section III gives a brief description of the ion thruster that is slated for testing in this facility, and Sections IV and V discuss the optical and electrical diagnostic methods, respectively, that are under development. Conclusions are presented in Section VI.

II. VACUUM FACILITY

A schematic of the vacuum chamber, jointly operated by The University of Tennessee and the Center for Advanced Space Propulsion, is shown in Fig. 1. The chamber has a steel shell that is 20 ft long and 9 ft in diameter. To establish the desired low vacuum

* This work was jointly supported by The University of Tennessee-Calspan Center for Advanced Space Propulsion under NASA grant NAGW 1195, Boeing Aerospace and Electronics, Seattle, WA and The University of Tennessee Space Institute, Tullahoma, TN.

** Calspan/CASP, Research Engineer
† UTSI/CASP, Research Engineer
‡ UTSI/CASP, Graduate Research Assistant
§ UTSI/CASP/CLA, Professor, ES&M

in the facility, a combination of mechanical pumps and cryopumps is used. Pumping the chamber down from atmospheric pressure to 10^{-3} Torr is achieved with a 150 ft³/min mechanical pump. Cryopumping of the system is achieved primarily by the helium cooled surface located inside the chamber. This cryosurface has an active area of about 36,000 in² (23 m²), and is cooled to about 20 K with a refrigeration unit capable of absorbing, at 20 K, a 900 W heat load. This cryopanel is surrounded with a liquid nitrogen cooled shroud, which is estimated to reach a maximum temperature of about 100 K. The main purpose of this shroud is to shield the heat radiated from the chamber walls.

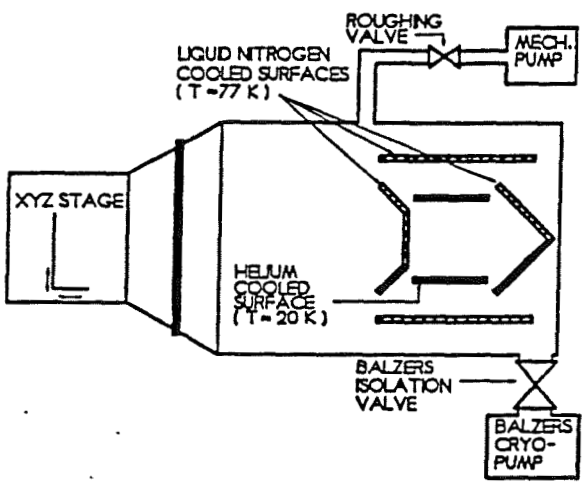

Fig. 1 *Schematic of vacuum chamber.*

To estimate the steady-state pumping capabilities of the cryopanel for a given gas flowing into the chamber, we have used the following equation [3]:

$$P_{ch} = \dot{m} \frac{\sqrt{2 \pi m k T_g}}{c A_c m}, \qquad (1)$$

where P_{ch} is the chamber pressure, $\dot{m}$ is the mass flow rate into the chamber, c is the fraction of gas particles that stick to the cryopanel, A_c is the surface area of the cryopanel, m is the atomic mass of the gas being pumped, k is Boltzmann's constant (1.38×10^{-23} J/K) and T_g is the gas temperature. Using Eq.(1), we calculate chamber pressures as a function of mass flow rate as shown in Fig. 2, where an argon propellant has been assumed. For this calculation, c was taken to be 0.9*0.75, where 0.9 is the sticking probability on the cryopanel [3], and 0.75 is the estimated fraction of cryopanel that will have gas condense on it; m = 6.68 x 10^{-26} kg; and T_g was either 300 K or 77 K as is illustrated in the plot. Although the exact gas temperature for particular operating conditions is yet to be determined, we estimate that it will be between that of the chamber walls (300 K) and that of the liquid nitrogen cooled shroud (77 K) for most applications.

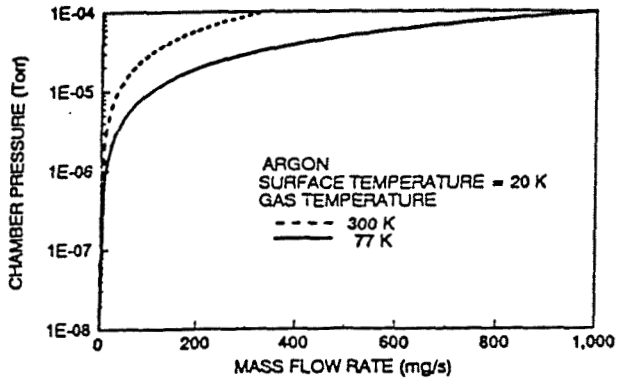

Fig. 2 *Estimated steady-state chamber pressure as a function of flow rate into the chamber.*

One limiting factor of the cryopanel is the heat load which the refrigeration unit can absorb while maintaining a temperature of 20 K. Equation 2 gives an estimate of this heat load Q_{cool} to the cryopanel as a function of the mass flow rate $\dot{m}$ into the chamber [3]:

$$Q_{cool} = \dot{m}[C_{pf}(T_v - T_c) + C_{pg}(T_g - T_v) + cE_a] + Q_{rad}. \qquad (2)$$

Here, C_{pf} is the specific heat for the cryodeposited frost (0.649 kJ/kg-K for argon [3]), C_{pg} is the specific heat for the pumped gas (0.520 kJ/kg-K), T_c is the cryopanel temperature (20 K), T_g is the gas temperature (assumed, here, to be 300 K), and T_v is the vapor sublimation temperature (50 K). Other parameters in Eq.(2) are c as defined above, E_a, the sum of the latent heats of fusion, vaporization and sublimation, for which a value of E_a = 16,300 kJ/kg was used [3], and Q_{rad}, the radiated heat load which was estimated to be 60 W by assuming a black body at 100 K. Figure 3 shows a plot of the required refrigeration power as a function of argon mass flow rate, obtained using Eq.(2). Noting that the heat load limit of the refrigeration unit is 900 W (while maintaining a helium temperature of 20 K), we thus

conclude that the maximum flow rate for these operating conditions is on the order of 60 mg/s for argon.

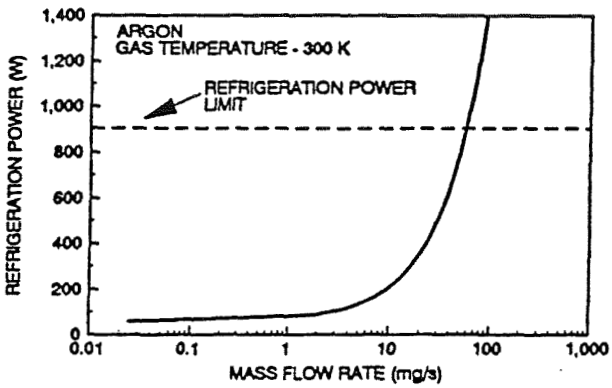

Fig. 3 *Required refrigeration input power versus mass flow rate into the chamber.*

In addition to the helium-cooled cryopump described above, the chamber is equipped with a 16 in. Balzers cryo-adsorption pump, also shown in Fig. 1. This pump is capable of pumping the lighter gases such as hydrogen that do not condense on the helium-cooled cryopanel. The pumping speed for the Balzers cryopump is given in table 1 for different gases. A 16 in. diameter air actuated vacuum valve is used to isolate this pump from the chamber.

Table 1 *Pumping speed of Balzers cryopump.*

	Pumping Speed (l/s)
Argon	5,500
Hydrogen	6,000
Nitrogen	6,500
Water	18,000

A computer program has been written to control and monitor the vacuum system. This program will be used to start the initial pump down of the chamber. When the chamber has reached a specified pressure, the program starts the cool-down of the liquid nitrogen shroud. This allows the user to let the computer start the chamber evacuation and cool-down cycles the night before a test, so that he/she can start the helium refrigeration system early in the morning upon arrival. The program then monitors a range of conditions in the chamber, and outputs these conditions to a computer screen and to a file for future reference.

A three dimensional translation stage (XYZ stage) has been installed inside the chamber as shown in Fig. 1. This stage will have the device of interest, for example, the ion thruster, mounted on it. The user can then position the device from outside the vacuum chamber using a computer control unit for the XYZ stage. This stage has a 12 inch reach in each of the three directions, and has a weight limit of 50 lbs.

III. ION THRUSTER

One of the proposed devices to be tested in the vacuum chamber is an ion thruster. Figure 4 gives a simple schematic of such a thruster, which, generally, is run either with xenon or argon as the propellant gas. The propellant enters the thruster from the left, and is ionized by electrons that are emitted from the (hollow) cathode, and subsequently drawn to the anode, located near the outside diameter of the thruster. These ions are then accelerated from inside the thruster through the grid system. The screen grid is maintained at either cathode or anode potentials. The potential of the accelerator grid is held several hundred volts negative relative to the screen grid. This acceleration process produces a thrust on the order of a fraction of a pound. However, specific impulses in excess of 2000 seconds can be obtained in this manner. The magnets on the inside of the thruster are used to confine the electrons and ions and help maintain the efficiency of the thruster. Since positive ions are extracted from the thruster, a neutralizer is located downstream of the thruster to introduce electrons into the ion beam so as to maintain charge neutrality.

Due to the small thrust of an ion thruster, these devices generally require operation times greater then 10,000 hours to accomplish a given mission, and the useful thruster lifetime becomes an issue of critical importance. For this reason, one important goal of our research is to develop sophisticated diagnostics that can help predict the lifetime of an ion thruster without running extended life tests. The proposed diagnostics are discussed in the following sections. A 30 cm diameter thruster shell, along with the required magnets, two sets of grids, and a cathode have been donated to CASP by NASA Lewis Research Center in Cleveland,

Ohio. The testing of the thruster will be conducted inside the vacuum chamber mentioned above. Necessary power supplies have been purchased, which will allow operation of the thruster with ion beam currents of up to 2 Amps and an electron current from the cathode to the anode of up to 15 Amps.

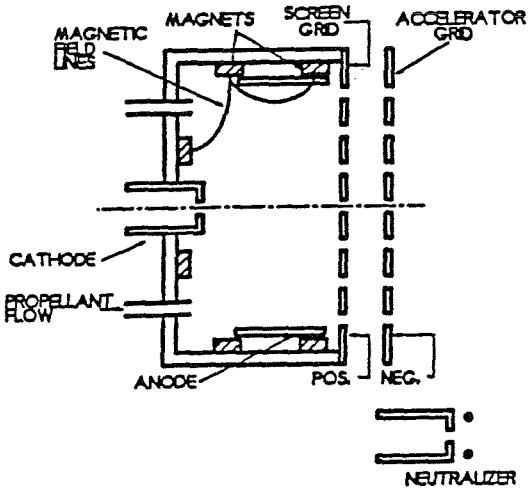

Fig. 4 *Schematic of an ion thruster.*

In order to predict the rise in background pressure in the vacuum chamber due to the operation of the ion thruster, the propellant flux for given operating conditions of the thruster must be known. In this regard, the thruster beam current is determined by the propellant flow through the thruster. This correlation is given by the following equation:

$$J_B \approx \frac{\dot{m}\, e\, \eta}{m}, \qquad (3)$$

where J_B is the beam current, $\dot{m}$ is the propellant flow rate, m is the mass of the propellant, e is the electronic charge, and η is the total propellant utilization efficiency. By rearranging Eq.(1), and incorporating it into Eq.(3), we then find the maximum allowable beam current for a given chamber pressure:

$$J_B \approx \frac{P_{ch}\, c\, A_c\, e\, \eta}{\sqrt{2\,\pi\, m\, k\, T_g}}. \qquad (4)$$

Some numerical results, obtained using Eq.(4), are shown in Fig. 5, which is a plot of the estimated beam current that can be obtained for a given chamber pressure. For this plot, η was taken to be 0.81, c = 0.68, T_g = 300 K and A_c = 0.75 x 23 m^2. Because, for optimal ion thruster operation, a facility pressure of less than 1 x 10^{-5} Torr is desired, Figure 5 implies that the thruster can be operated at beam currents up to 10 Amps.

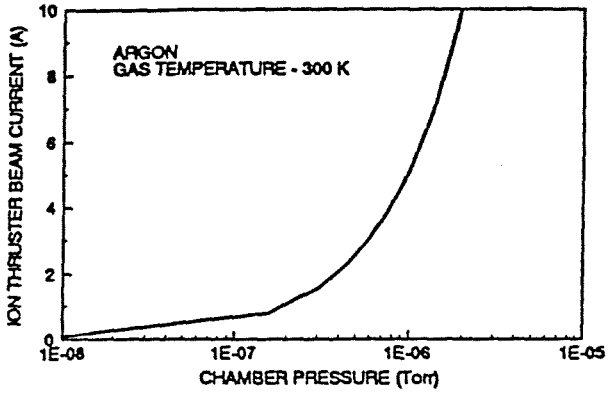

Fig. 5 *Ion thruster beam current that can be obtained as a function of chamber pressure.*

IV. OPTICAL DIAGNOSTICS

There are many candidate optical techniques that can be used to characterize flowfields in electrical propulsion systems. Of these, the primary one that we have singled out is that of laser induced fluorescence (LIF) [4]. In this technique, a laser beam is focused into the region of interest, exciting one of the species in the flow. Subsequently, fluorescence is detected, usually at right angles to the laser beam, by an optical detector, for example, a photo diode. The information that can be extracted from these LIF data includes temperature, density, and velocity components of the absorbing species along the laser beam. Furthermore, the technique is non-intrusive, and is capable of high spatial and temporal resolution. Some of the details of this method are discussed below.

First, Fig. 6 shows a schematic diagram of the experimental setup. A 10 Watt argon ion laser pumps a narrowband Coherent 699-21 ring dye laser, which is frequency stabilized to about 1 MegaHertz, or about 0.00002 Angstroms. This linewidth is much less than any other relevant broadening mechanism (Doppler,

Stark, pressure, power, and natural broadening), so, for all practical purposes, the laser can be regarded as a true single frequency source. The laser beam is then focused into the vacuum facility, and intersects the flow field at some predetermined position. Since the thruster is mounted on an XYZ positioning system, most optical components can be kept fixed, thereby simplifying optical alignment procedures, and the laser beam is scanned across the flowfield by translating the thruster instead. Because of the large size of the vacuum chamber, most critical optical components ate mounted inside the chamber, for example, to achieve optimum collection efficiency for the fluorescence radiation.

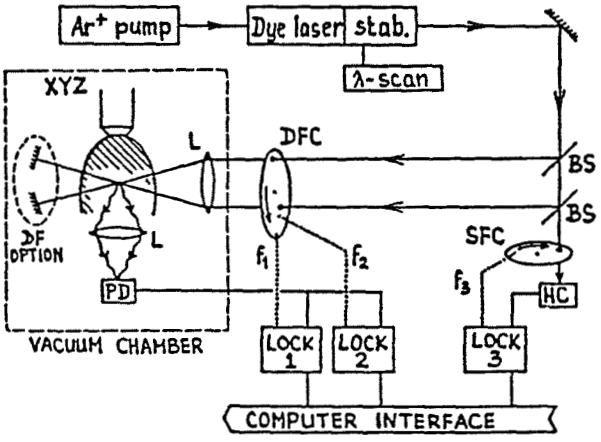

Fig. 6 *Schematic of optical diagnostics arrangement. BS = beam splitter; L = lens; PD = photo diode; HC = hollow cathode lamp; SFC/DFC = single/double frequency chopper, DF option = Doppler free option. LOCK = lockin detector. The thruster is mounted on an XYZ positioning system, while most optical components remain in fixed positions.*

To separate the LIF signal from background and plasma radiation in the flow, the laser beam is chopped, and all signals are measured with lockin amplifiers, which take the chopper frequency as reference (dotted lines in Fig. 6). Thus, great sensitivity is achieved. To measure more than one velocity component, the laser beam is split and recombined at a specified position in the flow.

The different laser paths are chopped at different frequencies (for example, with a dual frequency chopper as in Fig. 6), allowing, through determination of the associated Doppler shifts, the reconstruction of the velocity components of the absorbing state species at the probing point. Although only two velocity components can be extracted with the setup shown in Fig. 6, a three beam geometry could also be realized.

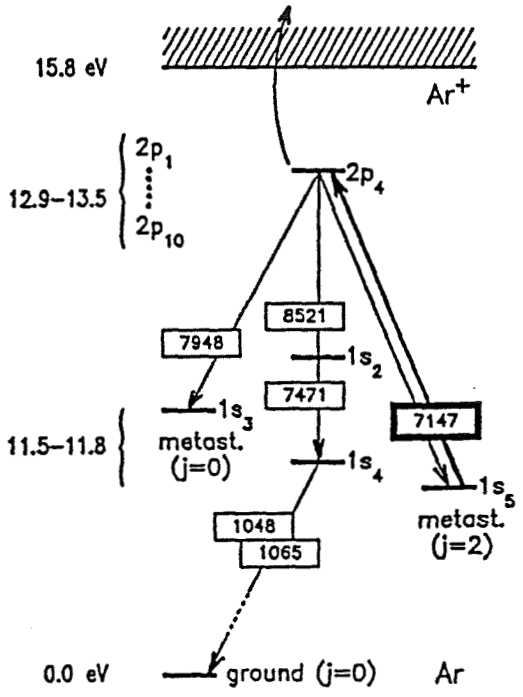

Fig. 7 *Partial energy level diagram of the argon atom, showing ground state, first and second excited states, and ionization continuum. Wavelengths in boxes are given in Angstroms. Excitation at 7147 Angstrom is shown as an example. Collisionally induced ionization from the 2p states plays an important role in the optogalvanic effect, while the fluorescence lines at 7147, 7471, 8521, and 7948 Angstroms form the basis for the LIF measurements.*

Unlike the well known laser Doppler velocimetry system, which relies on scattering of the laser light off of macroscopic particles in the flow, the LIF technique does not require seeding particulates into the flow, but relies instead on the resonant excitation of a specified ground state species naturally occurring in the flow. As an example, Fig. 7 shows part of the relevant energy level diagram of the neutral argon atom, which will be used as a propellant in our initial studies. Because argon, as do other noble gas atoms, has metastable states ($1s_3$ and $1s_5$ in Fig. 7 --- Paschen notation) that can be excited at optical wavelengths, the use of these metastable states as ground states for the LIF scheme

is particularly suited to LIF studies. Figure 7 shows how, for example, the $1s_5$ metastable state can be excited, at a wavelength of 7147 Angstrom, to one of the 2p states ($2p_4$ in Fig. 7), and how this state fluoresces back to the 1p states, and, by cascade emission in the far ultraviolet, to the neutral groundstate. In the LIF application, the fluorescence around 7000 to 8500 Angstroms, in particular, is detected and used to analyze the physical properties of the flowfield.

Because the fluorescence signal, at least for an optically thin plasma, is linearly proportional to the absorbing species density, relative density variations across a region of interest are easily monitored with LIF. More difficult is the extraction of absolute values for the density, which requires careful calibration of the entire optical system. Because the thruster flow is not expected to be in thermal equilibrium, the usual "Boltzmann plot" method is not applicable for the determination of plasma temperatures. Even for a nonequilibrium system, however, temperatures and velocities can, and will be measured, namely by measurements of the Doppler profiles of the absorbing species.

To measure such a Doppler profile, the wavelength of the laser is manually tuned to a particular absorption line of the gas. Subsequently, the laser is locked onto this line, and is frequency stabilized to within 1 MHz. Then, the laser is scanned electronically over a very narrow wavelength range around the linecenter. This range is typically several GigaHertz, sufficient to span the absorption line of interest. An example of such frequency (that is, wavelength) scans is shown in Fig. 8, which shows two simultaneous scans recorded in hollow cathode lamps (with argon buffer gas) at 7273 Angstroms ($1s_4$ to $2p_3$ transition). The two lines are 1.582 and 1.715 GHz wide, respectively, due to the combined effects of Doppler, Stark, natural, and power broadening. Although these measurements are preliminary, they indicate that, even for GigaHertz-wide lines, the linecenters can be determined to MegaHertz precision. For example, in Fig. 8, the two lines are Doppler shifted relative to each other by 10.5 MHz (that is, the shift is almost too small to be obvious by mere inspection of the figure), corresponding to a relative drift velocity of only 7.6 meters/sec. Thus, the capability for measuring velocity components in an electrical thruster to meters per second precision is established.

Actually, the data in Fig. 8 were obtained not with an LIF scheme, but by measuring the voltage change across the hollow cathode lamps as the laser is tuned through the absorption line. This method, known as optogalvanic spectroscopy [5], is very similar to LIF, except that, instead of measuring a fluorescence signal, one essentially measures an ionization signal. The mechanism behind this effect is illustrated schematically in Fig. 7: even though the final state of the laser absorption process is a neutral one ($2p_4$ in Fig. 7), collisional coupling with the plasma environment causes ionization of the gas (requiring only 2.5 to 3 eV), thereby changing the impedance of the discharge. Although optogalvanic spectroscopy is not, in itself, suitable for determination of the thruster flow parameters, it provides a very convenient reference for calibration of the velocity scale with regard to the Doppler profiles obtained with the LIF scheme. Indeed, although the linecenter of a GigaHertz wide line can be determined to MegaHertz precision, absolute determination of its center requires an absolute wavelength standard. Simultaneous measurement of the optogalvanic signal in a hollow cathode lamp provides just this standard.

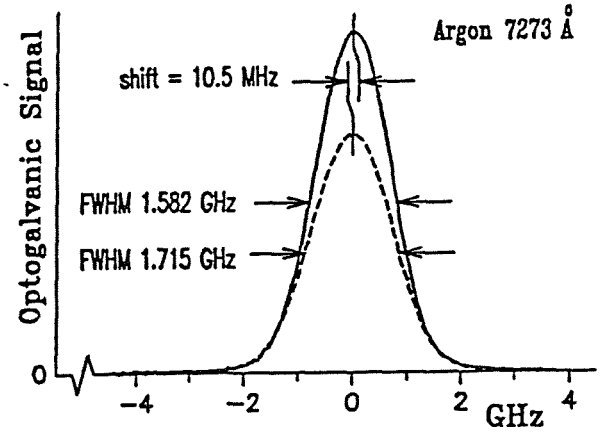

Fig. 8 *Simultaneous scans of the optogalvanic signal in copper (dashed curve) and uranium (solid curve) hollow cathode lamps with argon as buffer gas, revealing a relative Doppler shift of only 10.5 MHz in the presence of GigaHertz broadening.*

Figure 6 shows how this reference measurement is incorporated into the LIF scheme. Part of the laser beam is split off, chopped separately, and focused into a hollow cathode lamp, as the actual LIF measurement

on the thruster flow field takes place as described above. The optogalvanic signal from the hollow cathode lamp is then measured with a third lock-in detector, and is recorded simultaneously with the LIF signals from the other two lock-in detectors (one, two, or three detectors, depending on how many velocity components the LIF scheme is set up for). Thus, data are recorded similar to those in Fig. 8, where one of the profiles is known to be at exact linecenter, namely the optogalvanic one. From the shift of the LIF signal relative to the optogalvanic reference signal one can then determine the absolute velocity component of the absorbing species along the laser beam, and from the width of the Doppler profile one can extract the temperature. Again, it should be mentioned that this measurement can be performed at any position in the flow, thereby characterizing the flowfield with great accuracy.

Although we have described here the general principle of the LIF scheme, many additional details of the technique need to be addressed, for example, the determination of the various broadening mechanisms to the observed, composite, lineshapes. One powerful method, in this regard, is that of Doppler free LIF [6], or Doppler free optogalvanic spectroscopy [7]. Briefly, this technique consists of using overlapping, counterpropagating beams (for example, by reflecting the beams upon themselves, as indicated in Fig. 6). By carefully arranging the experiment, the LIF or optogalvanic signals then contain a component originating only from those atoms in the flowfield or in the lamp that experience equal Doppler shifts from the counterpropagating beams, that is, atoms with zero velocity. In this manner, inhomogeneous Doppler broadening can be eliminated, thereby rendering the purely homogeneously broadened lineshape. From this, we expect to be able to extract the Stark parameters of the line, yielding, among other parameters, values for the local electron density in the plasma [8]. Also, this method provides an independent check on the linecenter frequency calibration described above.

In conclusion, laser induced fluorescence will be used as the key optical diagnostic for spatially resolved measurements of density, temperature, and velocity of the thruster flowfield. Although we have used the example of an argon propellant here, the technique is readily extendable to other inert gases such as helium and xenon, or other species such as hydrogen and nitrogen.

V. ELECTRICAL DIAGNOSTICS

Although the nonintrusive nature of the optical diagnostics from Section IV are unparalleled by most other techniques, not all relevant plasma parameters are readily obtained from LIF data. In particular, the contribution from electrons is rather elusive to optical probes, since typical optical interactions in the visible region of the spectrum take place only in the much heavier neutral and ionized atomic species. Thus, to determine such parameters as plasma potential and electron density and temperature, one must generally rely on electric probes such as Langmuir probes and emissive probes. In addition, Faraday cages and retarding plate analyzers are electric probes that can be used for the determination of ion currents and ion energy distributions. Many excellent review articles on electric probes are available [9,10], and we will limit the discussion here to some of the salient features of these probes, and the extraction of plasma parameters from them.

In their simplest form, an electric probe (specifically, a Langmuir probe) consists of an insulated metal wire (perhaps with a small metallic sphere at the end) that is inserted into a plasma (that is, the thruster flowfield), and is connected to an electrical power supply. As the voltage on the probe is varied, the current to or from the probe is recorded as a function of the probe voltage. This measurement can either be made point by point, or the whole scan can be performed with a supply that is swept through the desired voltage range in a few microseconds. Furthermore, this measurement can be made at any position in the flowfield, by either maneuvering the probe, or, in our setup, by keeping the position of the probe fixed, and scanning the XYZ positioning system of the thruster. Unlike optical diagnostics, electrical probes can significantly modify the local plasma environment, and care must be taken in the interpretation of the data. If properly carried out, however, the details of the measured voltage-current characteristics can be related to the plasma parameters in the absence of the probe.

Figure 9 shows a typical voltage-current trace as obtained with a Langmuir probe. As the voltage V on the probe is varied, three distinct regions for the electron current I are manifest (labeled A, B, and C in Fig. 9). Region A, where the electron current saturates, marks the plasma potential V_p, where the probe voltage is equal to the plasma voltage. Similarly, region C,

where the ion current saturates, marks the floating potential V_f. At this floating potential, no current flows to or from the probe. The intermediate region, region B in Fig. 9, is the retarding field region, from which the electron temperature can be obtained from the slope of the signal in a singly logarithmic plot ("Boltzmann plot"). Finally, the electron density can be obtained from the magnitude of the probe current once the thermal electron velocity has been established.

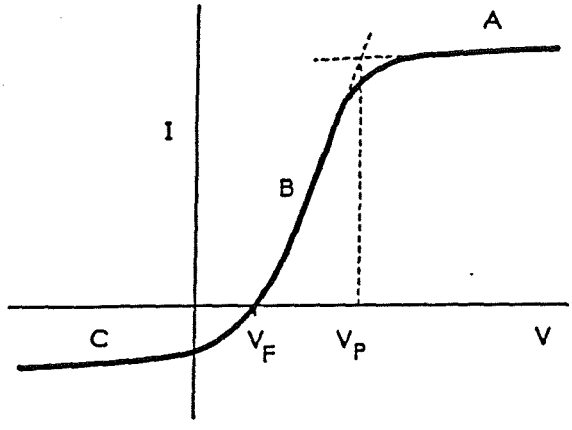

Fig. 9 *Typical voltage (V) - current (I) characteristic obtained with a Langmuir probe.*

An example of the extraction of these plasma parameters from Langmuir probe data is shown in Fig. 10. These data, which are discussed in more detail in Ref. [11], were taken in the downstream region (on axis) of a hollow cathode, electron source similar to those used in ion thrusters (the central leftmost part in Fig. 4 in Section III). In Fig. 10, the effects of different discharge currents on plasma potential, electron temperature, and electron density are all easily observed.

Of course, not all regions in a thruster are easily accessible to either electrical or optical probes. In particular, the sheath regions near the grids fall in this category, and we expect that the most fruitful approach in such regions is the input of experimentally determined upstream and downstream plasma parameters into numerical models, like the one described in the accompanying paper [2].

VI. CONCLUSIONS

A new 9 ft diameter by 20 ft long, cryogenically cooled vacuum facility at the University of Tennessee

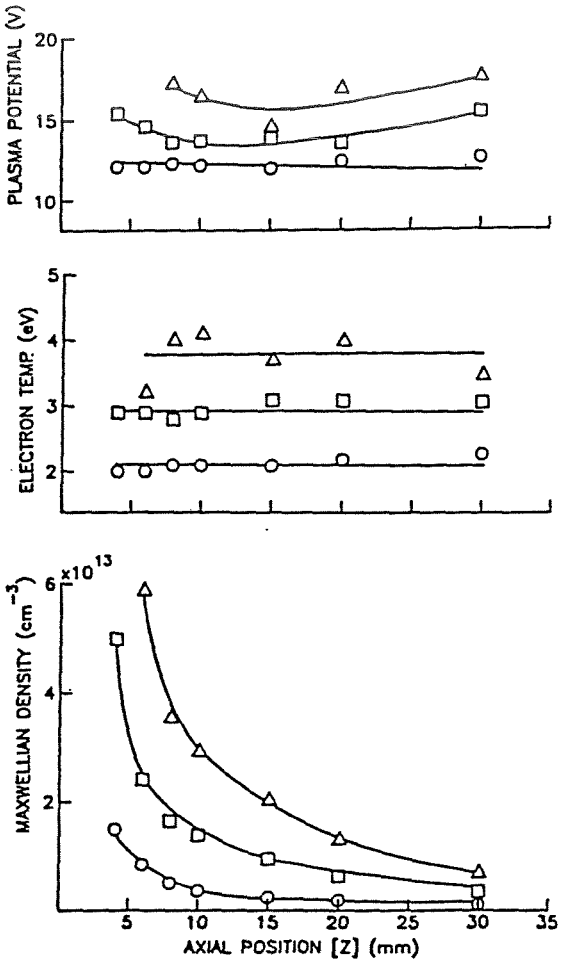

Fig. 10 *Data obtained with a Langmuir probe, on the centerline downstream of a hollow cathode. Circles, squares, and triangles are for discharge currents of 20, 40, and 60 Amps, respectively.*

Space Institute, jointly operated by the Center for Advanced Space Propulsion, has become operational. This facility will provide a baseline pressure of 10^{-7} Torr, and will allow for the testing of such electric propulsion devices as ion thrusters and arcjets at mass flow rates of up to 60 milligrams per second while maintaining a facility background pressure of 10^{-5} Torr. The first test, on a NASA supplied 30 cm diameter ion thruster, will commence shortly.

Apart from the evaluation of general thruster performance parameters such as gas flow and electrical characteristics, advanced optical and electrical diagnostics are under development. Specifically, laser induced fluorescence will be used to perform spatially resolved measurements of neutral gas density,

temperature, and velocity fields, and Langmuir probes will be used to obtain plasma potential contours and electron temperatures. The results of these tests should be instrumental to advance the understanding of the operation of these electric propulsion devices. For example, with precise experimental data on ion flowfield parameters as input for computational studies, a parallel effort on numerical modeling of the ion extraction dynamics in ion thrusters may, for the first time, yield accurate predictions for the grid erosion rates that are not easily obtained with ground testing alone.

ACKNOWLEDGMENTS

The contract monitor for this work was Dr. Jere Meserole of Boeing Aerospace and Electronics. We are grateful to NASA Lewis Research Center of Cleveland, Ohio for donating the ion thruster that will be used in these studies.

REFERENCES

[1] Rawlin, V. K., "Internal Erosion Rates of a 10-kW Xenon Ion Thruster," AIAA Paper 88-2912, AIAA/ASME/SAE/ASEE 24th Joint Propulsion Conference, Boston, MA, July 11-13, 1988.

[2] Peng, X., Ruyten, W. M., Friedly, V. J., and Keefer, D., "Plasma Particle Simulation of Electrostatic Ion Thrusters," this symposium, Tullahoma, Tennessee, November 1990.

[3] Tempelmeyer, K. E., *Heat Transfer at Low Temperatures*, ed. by Frost, W. (Plenum, New York, 1975), pp. 213-227.

[4] Ruyten, W. M., "Aspects of laser induced fluorescence employing pulsed and modulated excitation," Ph.D. thesis, the University of Tennessee, Knoxville, August 1989.

[5] Keller, R. A., and Zalewski, E. F., Appl. Opt. **19**(19), 3301 (1980), and references therein.

[6] Letokhov, V. S. and Chebotayev, V. P., *Nonlinear Laser Spectroscopy* (Springer, Berlin, 1977), Chap. II.

[7] Lawler, J. E., et al., Phys. Rev. Lett. **42**(16), 1046 (1079).

[8] Copley, G. H. and Cam, D. M., J. Quant. Spectr. Rad. Transf., **14**, 899 (1974); see also Griem, H. R., *Plasma Spectroscopy* (McGraw Hill, New York, 1964).

[9] Chen, F. F., in *Plasma Diagnostic Techniques*, ed. by Huddlestone, R. H., and Leonard, S. L. (Academic, New York, 1965), p.113.

[10] Hershkowitz, N., in *Plasma Diagnostics*, Vol. 1, ed. by Auciello, O., and Flamm, D. L. (Academic, New York, 1989), p.113.

[11] Friedly, V. J. and Wilbur, P. J., "High Current Hollow Cathode Phenomena," AIAA paper 90-2587, Orlando, Florida, July 1990; Friedly V. J., "Hollow Cathode Operation at High Discharge Currents," NASA report CR-185238, April 1990.